Collective cyclotron modes in high-mobility two-dimensional hole systems in GaAs - (Ga, Al)As heterojunctions: I. Experiments at low magnetic fields and theory

1997 J. Phys.: Condens. Matter 9 3163

(http://iopscience.iop.org/0953-8984/9/15/009)

J. Phys.: Condens. Matter **9** (1997) 3163–3179. Printed in the UK PII: S0953-8984(97)79733-9

Collective cyclotron modes in high-mobility two-dimensional hole systems in GaAs–(Ga, Al)As heterojunctions: I. Experiments at low magnetic fields and theory

B E Cole†, F M Peeters‡‖, A Ardavan‡, S O Hill‡¶, J Singleton‡+, W Batty§, J M Chamberlain†, A Polisskii‡, M Henini† and T Cheng†

† Department of Physics, The University of Nottingham, Nottingham NG7 2RD, UK

‡ Department of Physics, University of Oxford, Clarendon Laboratory, Parks Road, Oxford OX1 3PU, UK

§ Department of Electronics, University of York, Heslington, York YO1 5DD, UK

Received 21 November 1996, in final form 14 February 1997

Abstract. The cyclotron resonance of very high-mobility two-dimensional holes in GaAs–(Ga, Al)As heterojunctions grown on (111), (311) and (100) substrates has been studied over the frequency range 30 to 200 GHz. Although the presence of two hole spin subbands in the samples suggests that two cyclotron resonances should be observed, in practice only a single resonance occurs for a wide range of conditions (temperature, field) and sample properties (hole density, mobility). Furthermore, the cyclotron resonance spectra often exhibit a strong temperature dependence. In the case of a single, sharp cyclotron resonance, the resonance field may shift by as much as 20% when warming the sample from 1.4 to 4.2 K. In the case of spectra containing multiple cyclotron resonances, similar changes in temperature shift the resonance positions together to form a single cyclotron absorption. This behaviour is explained in terms of two interacting hole subsystems with different effective masses formed by the two spin subbands. An analytical expression for the contribution to the high-frequency conductivity due to coupled cyclotron motion of the two hole systems is derived and shown to encompass previous theories developed for more restricted ranges of conditions. The expression predicts the complex behaviour of the experimental spectra very well, and enables hole masses, hole–lattice scattering rates and hole–hole scattering rates to be extracted. Comparisons between theory and data also show that a reactive interaction dominates the coupling between the spin subsystems at low temperatures. This is the first of two papers dealing with correlated hole cyclotron resonance; the second shows that the model derived in this work can also be used to treat cyclotron resonance data recorded at very high magnetic fields ∼40 T.

1. Introduction

The two-dimensional hole system (2DHS) formed in GaAs–(Ga, Al)As heterostructures provides a fascinating contrast to the equivalent electron system. Whereas the latter possesses an almost parabolic dispersion relationship and a Pauli spin splitting which is

‖ Permanent address: Departement Natuurkunde, Universiteit Antwerpen (UIA), Universiteitsplein 1, B-2610 Antwerpen, Belgium; e-mail: peeters@uia.ua.ac.be.

¶ Permanent address: National High Magnetic Field Laboratory, 1800, East Paul Dirac Drive, Florida State University, Tallahassee, FL 32306-4005, USA.

+ Author to whom any correspondence should be addressed; e-mail: J.Singleton1@physics.ox.ac.uk.

0953-8984/97/153163+17$19.50

much less than the cyclotron energy, the 2DHS exhibits a wide range of effective masses, a large and complex non-parabolicity and a relatively large energy splitting of the hole spin states at finite wavevector in the absence of an applied magnetic field. Furthermore, all of these characteristics may be varied by adjustment of substrate orientation and/or confinement length [1–3]. In view of the very non-parabolic hole Landau levels, adjacent cyclotron resonance (inter-Landau-level) transitions may have very different energies, so when several Landau levels are populated, the occurrence of more than one cyclotron resonance seems likely; e.g. in the limit of very low fields, two resonances representing the classical cyclotron motion of holes in the two 'spin subbands' might be expected. However, with the exception of a small number of early studies of relatively low-mobility 2DHS, which did exhibit multiple cyclotron resonances [4], more recent experiments on higher-mobility samples have revealed single, sharp resonances, even when several Landau levels are populated [1, 5]. In order to clarify the origin of this phenomenon, we have carried out measurements of the cyclotron resonance of two-dimensional holes in GaAs–(Ga, Al)As heterojunctions over the frequency range 25 GHz to 200 GHz, corresponding to magnetic fields of less than 5 T. The cyclotron resonance spectra have been observed as a function of temperature T, areal hole density p_s and hole mobility μ; over the frequency range chosen, both the cyclotron energy ($\hbar\omega_c$) and kT are less than the Fermi energy (E_F) for most of the samples studied [6].

These measurements have allowed some criteria for the observation of multiple or single cyclotron resonances to be deduced. The experiments involving variation of temperature are especially important in this context, as they enable the multiple–single-cyclotron-resonance boundary to be crossed. Furthermore, when only a single resonance is observed, a strong temperature dependence of the cyclotron resonance field is apparent. This effect is remarkably robust, and has been observed in magnetic fields of up to 40 T and for temperatures of up to 20 K (see reference [7]).

As the two-dimensional hole system consists of two sets of interacting holes (the two spin subbands) with differing effective masses, we have based our analysis of the data on an extension of semiclassical models originally derived for two-component systems such as electrons in Si MOSFETs; in the latter case the two components represented the different X valleys of Si. An analytical expression for the contribution to the high-frequency conductivity due to coupled cyclotron motion of the two hole systems has been derived. This expression is shown both to encompass previous calculations and to predict the complex behaviour of the experimental spectra. Using a comparison of model and experiment, the hole effective masses, hole–lattice scattering rates and hole–hole scattering rates are extracted.

This paper is organized as follows: the experimental arrangements and sample details are given in section 2. The main experimental data are presented in section 3. In section 4 the semiclassical expression is derived; section 5 illustrates its use to extract parameters from the experimental data. A summary is given in section 6. This is the first of two papers dealing with correlated hole cyclotron resonance; in the second [7], the model derived in this work is applied to cyclotron resonance data recorded at very high magnetic fields ∼40 T.

2. Experimental details

The heterojunctions used in this study were grown under similar conditions on the crystal planes (100), (311)A and (111) of GaAs by molecular beam epitaxy [8] and had the following layer structures: 170 Å GaAs cap layer, 400 Å doped (10^{18} cm^{-3}) $Al_{0.33}Ga_{0.67}As$, undoped $Al_{0.33}Ga_{0.67}As$ spacer, 5000 Å undoped GaAs, superlattice buffer, semi-insulating

Table 1. Sample identification, growth and DC transport characteristics.

Sample No: I.D.	Growth direction	2 K mobility **(**$m^2\ V^{-1}\ s^{-1}$**)**	Total hole density ($10^{15} m^{-2}$)	Spacer layer thickness (nm)
1: NU939	(311)A	9	3.3	20
2: NU877	(100)	14	2.8	45
3: NU942	(311)A	120	0.8	60
4: NU950	(111)	10	3.0	45
5: NU1172	(311)A	100	0.4	120

substrate. Spacer layer thicknesses, p_s and low-temperature mobilities μ derived using the Hall and Shubnikov–de Haas effects are given in table 1. The sample substrates were thinned to less than 100 μm prior to the experiments.

A Millimetre-wave Vector Network Analyser [9] (MVNA) was used as source and detector of the millimetre-wave radiation (25–200 GHz) for the cyclotron resonance measurements. The MVNA was set at a fixed frequency as the magnetic field $\boldsymbol{B}$, provided by a superconducting solenoid, was swept. Many of the cyclotron resonance spectra were recorded by measuring the transmission of the thinned sample, which could be maintained at a stable temperature between 1.4 and 4.2 K using ^{4}He exchange gas. However, further measurements of mm-wave power absorption were made using a cylindrical resonant cavity, tunable from 50–70 GHz; this provides a well controlled electrodynamic environment for the sample. Ideally, the measured cavity transmission amplitude is determined by the absorption of the sample, i.e. the real part of the dynamical conductivity, $\mathrm{Re}\{\sigma(\omega)\}$, and the phase of the transmitted signal is determined by the dispersion, $\mathrm{Im}\{\sigma(\omega)\}$. Since the millimetre-wave source is locked to a quartz oscillator, there is in practice a small amount of mixing (<30%) between the absorption and the dispersion. This mixing is reflected in the experimental cyclotron resonance spectra [10]. The cavity measurements were carried out in a single-shot ^{3}He insert which allowed the sample temperature to be varied in the range 0.50–4.2 K.

3. Experimental cyclotron resonance data

In this section we shall seek to display the (at first sight complicated) phenomenology of the cyclotron resonance spectra of the two-dimensional holes, prior to the quantitative analysis in section 4. Figures 1(a) and 1(b) show the cavity transmission for samples 1, 2 and 3 as a function of magnetic field at frequencies of 53.4 GHz (figure 1(a)) and 67 GHz (figure 1(b)); all data were recorded at 1.4 K. Both sample 1, a (311)A orientation sample of relatively low mobility and high hole density (table 1), and sample 2, a (100) orientation sample of similar hole density but somewhat higher mobility, exhibit two clear cyclotron resonances, seen as minima in the cavity transmission. At such frequencies, both $\hbar\omega_c$ and kT are much less than the Fermi energies of samples 1 and 2 ($E_F \sim 3$ meV), so resonances associated with the two spin subbands of different mass might be expected. By contrast, only a single sharp resonance is observed at these two frequencies for sample 3, a (311)A orientation sample of lower hole density and very high mobility (table 1).

Figure 1(c) shows the effect of increasing the cyclotron frequency to ∼190 GHz; in this case the traces represent straightforward transmission, without the use of a cavity [11]. Sample 1 shows a more complicated cyclotron resonance lineshape comprising three resonances; no distinction in terms of spin subbands can be made here. However, sample 2

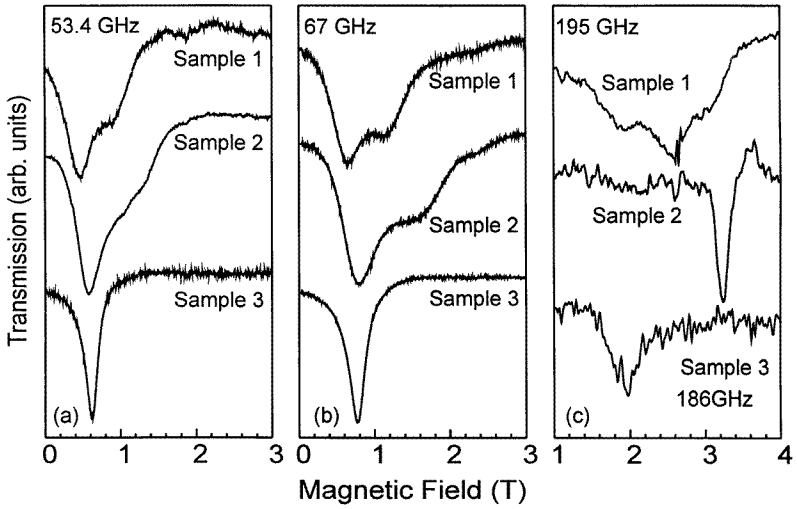

Figure 1. Resonant cavity spectra at the frequencies 53.4 GHz (a) and 67.0 GHz (b) and magnetotransmission spectra (c) for samples 1, 2 and 3 at 1.4 K.

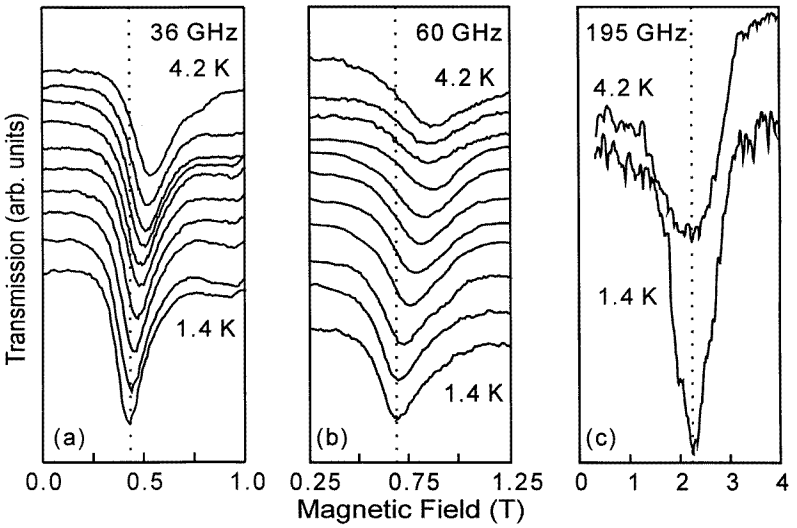

Figure 2. Magnetotransmission spectra for sample 5 at a range of temperatures. In each case the vertical scale is transmission, measured in arbitrary units; traces are shown at various constant temperatures between 4.2 K (topmost trace) to 1.4 K (lowest trace). For (a), (b) and (c), the frequencies are 36 GHz, 60 GHz and 195 GHz respectively.

displays a single, sharpened resonance with no clear multi-line structure. A single cyclotron resonance is also observed in the case of sample 3.

When a single cyclotron resonance is observed, its position is often found to be very temperature dependent. The temperature dependence of the cyclotron resonance for a very low-p_s sample (sample 5) is shown in figure 2 at three frequencies; the data represent simple transmission measurements. The lower-frequency (i.e. lower-field) cyclo-

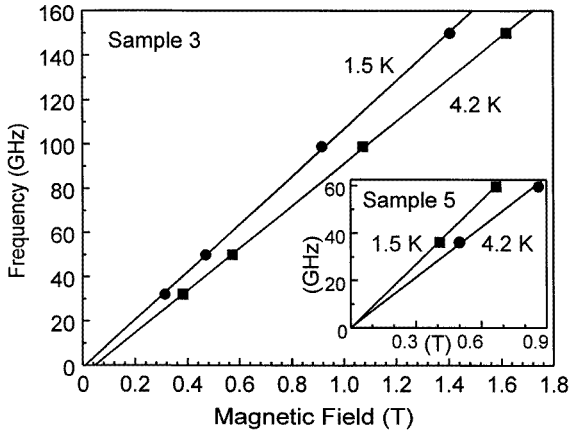

Figure 3. A plot of the cyclotron frequency as a function of magnetic field for sample 3 at 1.4 K and 4.2 K. The solid line is a linear fit to the points. The inset shows the cyclotron frequency plotted against magnetic field for sample 5 at 1.5 K and 4.2 K.

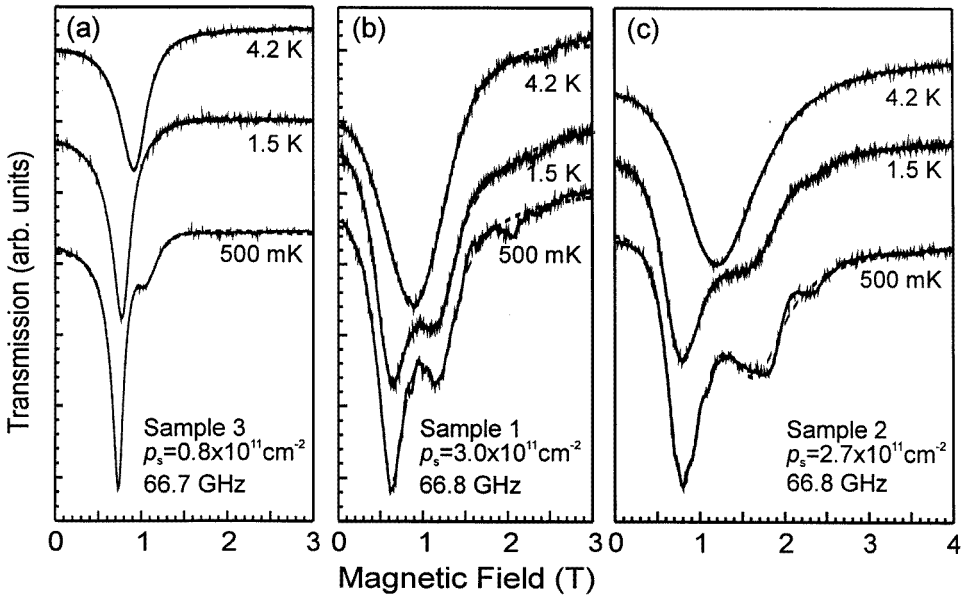

Figure 4. Resonant cavity spectra of samples 3 (a) (66.7 GHz), 1 (b) (66.8 GHz) and 2 (c) (66.8 GHz) at temperatures of 500 mK, 1.5 K and 4.2 K.

tron resonances (figures 2(a) and 2(b)) exhibit a strong shift with temperature; however, once the ultraquantum limit is reached (figure 2(c)), no shift is discernible between 1.4 and 4.2 K (however, see reference [7], in which a shift of the resonance to lower fields with increasing temperature appears at higher fields and temperatures). Figure 3 shows the cyclotron frequencies of samples 3 (main figure) and 5 (inset) plotted against resonant field for temperatures of 1.4–1.5 K and 4.2 K; the data show that the upshift in cyclotron resonance field with temperature is proportional to the frequency, indicating that it corresponds to an

increase in measured cyclotron mass, rather than, say, the temperature-dependent depinning of a quasi-bound state [12]. Such upshifts of cyclotron resonance field have been found to be a general feature of hole cyclotron resonance spectra and have been observed in many samples not detailed in this report, covering a range of p_s from 0.4×10^{15} m^{-2} to 2×10^{15} m^{-2}, and both (311)A and (100) substrate orientations [3, 13].

The evolution of the cyclotron resonance lineshape with temperature is illustrated in figure 4 for samples 1, 2 and 3 (cf. figure 1); all data in this figure were recorded with the samples in the resonant cavity. At 4.2 K a single Lorentzian lineshape is observed in all cases. As the temperature is lowered to 1.5 K, the single cyclotron resonances in the two higher-density samples (1 and 2; figures 4(b) and 4(c)) split into two. A further decrease of the temperature to 500 mK results in extra structure superimposed on the transmission spectra of samples 1 and 2 (figures 4(b) and 4(c)); the frequency independence of this structure and its periodicity in $1/B$ (see also figure 6, below) show that it is due to quantum oscillations [14], well known in two-dimensional electron systems. At 500 mK, even the lowest-density sample (3; figure 4(a)) develops a second, weak resonance on the high-field side of the main resonance.

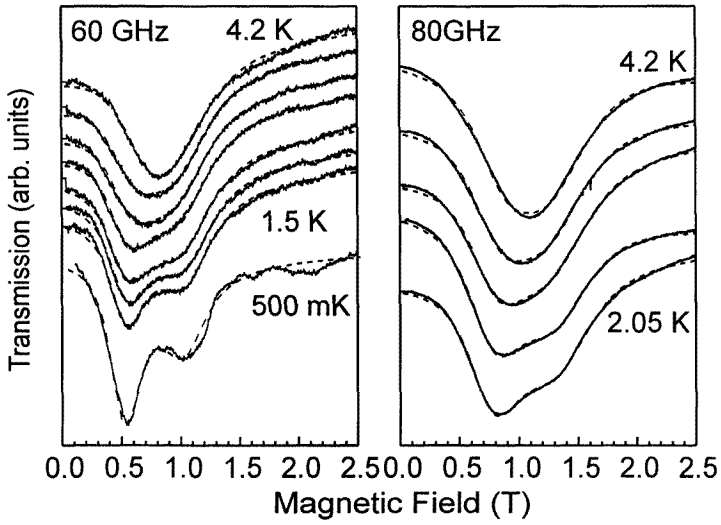

Figure 5. The resonant cavity magnetotransmission of sample 1 over a range of temperatures at 60 GHz (a) and 80 GHz (b). Experimental data are shown as solid lines; fitted lineshapes (see sections 4 and 5 of the text) have been plotted as dotted lines.

Figure 5 shows the evolution of the cyclotron lineshape with temperature in more detail; it features cavity measurements of sample 1 at 60 GHz and 80 GHz. The two cyclotron resonance fields shift together as the temperature is raised; it is worth pointing out that the lineshapes measured at 4.2 K cannot be modelled by simply broadening the lower-temperature double resonances.

The frequency dependence of the cyclotron resonance lineshapes was studied over the tunable range of the resonant cavity, ∼50–70 GHz. The small, higher-field resonance observed for sample 3 at 500 mK (figure 4(a)) was found to increase in strength with increasing frequency, as shown in figure 6(a). Similar data are shown for the higher-density sample 3 in figure 6(b); although the change in the relative strength of the two cyclotron resonances is less marked, the field independence of the quantum oscillation features is

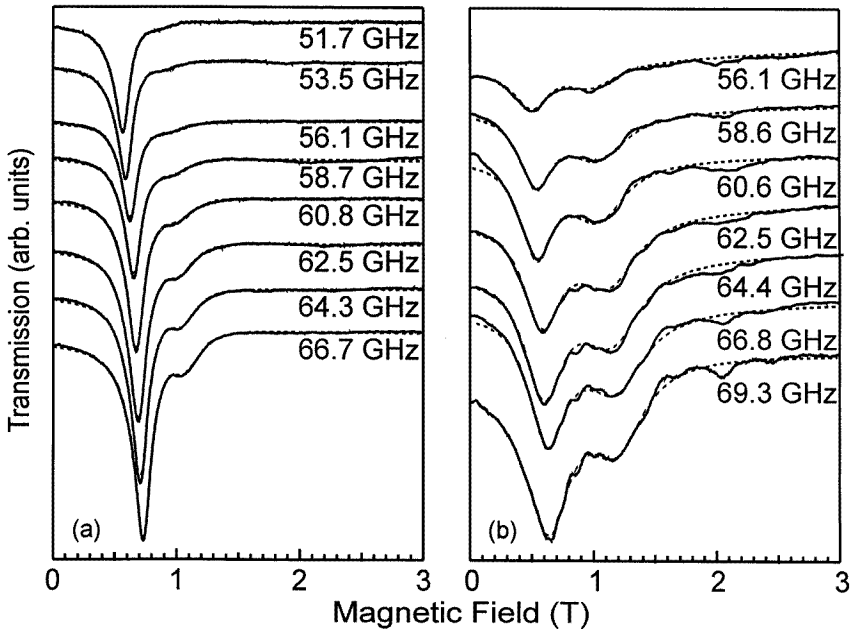

Figure 6. The frequency dependence of the cyclotron resonance spectra of samples 3 (a) and 1 (b), measured in the tunable resonant cavity. In all cases the sample temperature is 500 mK. The fitted lineshapes are plotted as dotted lines. The frequencies are indicated by each trace.

clearly demonstrated.

4. Theory of cyclotron resonance in a two-component interacting system

Cyclotron resonance studies of the two-carrier system formed by electron pockets in the different X valleys of Si MOSFETs show some striking parallels with the results reported in section 3 of this paper. In the Si work, frequently a single resonance was observed, despite a significant population of electrons in both valleys [15]. In addition, a strong temperature dependence of the resonance position was observed. In order to explain these phenomena, Coulomb interactions between the two electron populations were examined in a number of studies. Appel and Overhauser [16] showed, using a classical model, that electron–electron scattering could relax the relative momentum between two electron populations undergoing cyclotron orbits of different frequencies. In the limit of strong electron–electron scattering, a single coupled resonance, lying at the mean frequency of the two 'independent' cyclotron resonances, was predicted. This model was only valid in the low-field regime, where $\bar{h}\omega \ll E_F$. In the remaining part of this section, we shall apply these ideas to the two-component hole system, and derive a model which encompasses all of the experimental regimes encountered.

Kohn's theorem [17] states that in a translationally invariant system the cyclotron resonance absorption is not influenced by carrier–carrier interactions. This theorem is also applicable to systems which are confined by parabolic confinement potentials [18]. The consequences of this theorem are far reaching; it allows one to replace the many-particle system by a single effective particle. However, in the presence of disorder or a non-parabolic

dispersion relation, or different types of carrier with e.g. different masses, Kohn's theorem is no longer valid and inter-particle interactions can alter the cyclotron resonance absorption spectrum (see reference [18] and references therein).

For small magnetic fields and small-to-moderate hole densities, the two dimensional hole systems studied in this paper in effect contain two different hole subsystems (the spin subbands), which we label using the index $i = 1, 2$. The subsystems are characterized by the parameters n_i, m_i and τ_i, where n_i is the hole density, m_i is the hole mass and τ_i is the relaxation time of the ith subsystem. Following Kukkonen and Maldague [19] we introduce $\boldsymbol{P}_i$, the total momentum of each subsystem, and define $\boldsymbol{P} = \boldsymbol{P}_1 + \boldsymbol{P}_2$ as the total momentum and $\boldsymbol{\Pi} = (\boldsymbol{P}_1/n_1m_1 - \boldsymbol{P}_2/n_2m_2)n_1n_2m_1m_2/(n_1m_1 + n_2m_2)$ as the relative momentum of the two subsystems. Because $\boldsymbol{P}_1 = \boldsymbol{\Pi} + \boldsymbol{P}n_1m_1/(n_1m_1 + n_2m_2)$ and $\boldsymbol{P}_2 = -\boldsymbol{\Pi} + \boldsymbol{P}n_2m_2/(n_1m_1 + n_2m_2)$, the total current of the system is given by

$$\boldsymbol{J} = \frac{e}{A}\left(\frac{n_1 + n_2}{n_1m_1 + n_2m_2}\boldsymbol{P} + \left(\frac{1}{m_1} - \frac{1}{m_2}\right)\boldsymbol{\Pi}\right). \tag{1}$$

This not only depends on the total momentum $\boldsymbol{P}$, but also, when $m_1 \neq m_2$, on the relative momentum $\boldsymbol{\Pi}$ of the two-carrier system. It is the latter which is responsible for the dependence of the current (and thus the conductivity and the cyclotron absorption) on the carrier–carrier interaction.

We solved the kinetic equations of motion and assumed that the time dependence of the relative momentum is given by

$$\frac{\mathrm{d}\boldsymbol{\Pi}}{\mathrm{d}t} = -\left(\mathrm{i}\omega_0 + \frac{1}{\tau_{12}}\right)\boldsymbol{\Pi} \tag{2}$$

where the frequency ω_0 and the relaxation time τ_{12} are determined by the Coulomb interaction between the two subsystems. Thus the inter-particle interaction can be resolved into reactive (i.e. oscillating) and dissipative (i.e. decaying) parts in the time dependence of the relative momentum. In general one has $\mathrm{d}\boldsymbol{\Pi}/\mathrm{d}t = -\mathrm{i}M(\omega)\boldsymbol{\Pi}$, where $M(\omega)$ is a memory function which also depends on the frequency ω of the applied light to which the system responds. Although the imaginary part of the interaction was ignored in the calculations of reference [16], the memory function was calculated by Ting *et al* [20] for the case of Coulomb scattering between electron pockets in different X valleys of a Si MOSFET. In the present approach we take $M(\omega) = \omega_0 - \mathrm{i}/\tau_{12}$. This is a generalization of the work by Appel and Overhauser [16] who assumed a purely dissipative relaxation of the electron momentum. While Takada and Ando [21] used an approach which is more closely related to the present one, with a real and imaginary part, their final expression for the conductivity is slightly different.

The solution of the kinetic equations proceeds along the lines given by Appel and Overhauser [16] and therefore we shall limit ourselves to the main results. We assume that a magnetic field is applied perpendicular to the 2D plane and that we are interested in the linear response to circularly polarized light with frequency ω, $J_x + \mathrm{i}J_y = \sigma(\omega)(E_x + \mathrm{i}E_y)$. The final result is

$$\begin{aligned}\sigma(\omega) = \frac{e^2}{D(\omega)}\Bigg\{&\mathrm{i}\left(\omega - \omega_{c,1} - \frac{\mathrm{i}}{\tau_1} - f_1\left(\omega_0 + \frac{\mathrm{i}}{\tau_{12}}\right)\right)\frac{n_2}{m_2} \\ &+ \mathrm{i}\left(\omega - \omega_{c,2} - \frac{\mathrm{i}}{\tau_2} - f_2\left(\omega_0 + \frac{\mathrm{i}}{\tau_{12}}\right)\right)\frac{n_1}{m_1} \\ &- \mathrm{i}\left(\omega_0 + \frac{\mathrm{i}}{\tau_{12}}\right)\frac{2n_1n_2}{n_1m_1 + n_2m_2}\Bigg\}\end{aligned} \tag{3}$$

where

$$D(\omega) = -\left(\omega - \omega_{c,1} - \frac{\mathrm{i}}{\tau_1} - f_1\left(\omega_0 + \frac{\mathrm{i}}{\tau_{12}}\right)\right)\left(\omega - \omega_{c,2} - \frac{\mathrm{i}}{\tau_2} - f_2\left(\omega_0 + \frac{\mathrm{i}}{\tau_{12}}\right)\right) + f_1 f_2\left(\omega_0 + \frac{\mathrm{i}}{\tau_{12}}\right)^2 \tag{4}$$

with $f_1 = 1/(1+n_1m_1/n_2m_2)$ and $f_2 = 1/(1+n_2m_2/n_1m_1)$ and where we have introduced the single-particle cyclotron frequencies $\omega_{c,i} = eB/cm_i,\ i = 1, 2$. The absorption is given by the real part of equation (3), i.e. $\mathrm{Re}\{\sigma(\omega)\}$. For light circularly polarized in the other sense, i.e. $E_x - \mathrm{i}E_y$, the result is similar to equation (3) except that $\omega_{c,i}$ must be replaced by $-\omega_{c,i}$.

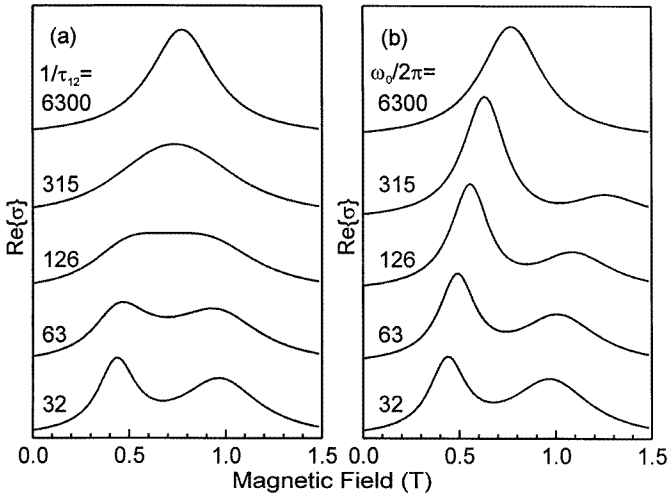

Figure 7. The real part of the dynamical conductivity of a two-component Fermi liquid, calculated according to the model described in the text for a range of hole–hole scattering rates. The parameters used are as follows: $\omega/2\pi = 60$ GHz, $m_1 = 0.21m_e$, $m_2 = 0.46m_e$, $1/\tau_1 = 1/\tau_2 = 94$ GHz, $n_2/n_1 = 1.75$. (a) shows the effect of the resistive component of the hole–hole interaction; the values indicate $1/\tau_{12}$ and ω_0 is set to zero. (b) shows the effect of the reactive component of the hole–hole interaction; $1/\tau_{12}$ is set to zero and the values indicate $\omega_0/2\pi$.

The contrasting way in which the real part, $1/\tau_{12}$, and the imaginary part, $\omega_0/2\pi$, of the hole–hole interaction influence the cyclotron resonance lineshape is illustrated in figures 7(a) and 7(b), which show $\mathrm{Re}\{\sigma(\omega)\}$, evaluated at $\omega = 60$ GHz, for purely real and purely imaginary hole–hole interactions respectively. The remaining input parameters are listed in the figure caption. $1/\tau_{12}$ acts to relax the relative momentum, so reducing the splitting between the two single-particle resonances. This resistive interaction provides an internal mechanism for dissipation which may broaden the cyclotron resonance linewidth significantly, however high the DC mobility. $\omega_0/2\pi$, by contrast, shifts the balance of oscillator strength between the two resonances while renormalizing their masses. $\omega_0/2\pi$ always acts to shift both resonances to higher field and increase their splitting; by shifting the oscillator strength to the lower-field resonance the mean cyclotron resonance mass of the system is made to remain unaltered, as required by Kohn's theorem.

The present result has already been related to the models derived in the 1970s and 1980s [16, 20] to describe the behaviour of the cyclotron resonance in Si MOSFETs [15].

It is easy to show that the above formula reduces to the one-component cyclotron resonance result in the limit of $m_1 = m_2$, $\tau_1 = \tau_2$, and $\omega_0 = 0$, $\tau_{12} = \infty$. For $\tau_{12} = \infty$ and $\omega_0 = 0$ two cyclotron resonance peaks are found centred at $\omega_{c,1}$ and $\omega_{c,2}$ respectively. It is well known that Coulomb scattering results in a carrier relaxation rate which is proportional to T^2 for $E_F > k_B T$. Consequently, for sufficiently high temperatures and in the absence of any reactive coupling (i.e. $\omega_0 = 0$) we can take the limit $\tau_i/\tau_{12} \gg 1$ which leads to the strong-coupling result with a single Lorentzian CR peak

$$\sigma(\omega) = -\mathrm{i}e^2 \frac{(n_1 + n_2)^2}{n_1 m_1 + n_2 m_2} \frac{1}{\omega - \omega_c + \mathrm{i}/\tau} \tag{5}$$

with the CR frequency $\omega_c = (n_1 m_1 \omega_{c,1} + n_2 m_2 \omega_{c,2})/(n_1 m_1 + n_2 m_2)$ and the broadening $1/\tau = (n_1 m_1/\tau_1 + n_2 m_2/\tau_2)/(n_1 m_1 + n_2 m_2)$. Thus with increasing temperature the CR spectrum evolves from two peaks to a single peak.

Recently, the high-field cyclotron resonance of high-mobility GaAs heterostructures has been measured by a number of groups [22] in the quest for evidence of Wigner crystallization. For low Landau-level filling factors, a single cyclotron resonance was observed at extremely low temperatures; with increasing temperature this split into two resonances. This behaviour is the opposite of that observed at low magnetic fields in the hole systems studied in the present paper (see e.g. figure 4). The high-field behaviour of the two-dimensional electron systems was explained by Cooper and Chalker [23] as resulting from a crossover from independent spin-split resonances to a single cyclotron mode dominated by Coulomb interactions. In this case it is band non-parabolicity which provides the two subsystems of carriers with different mass; i.e. the masses of the electrons in the spin-up and spin-down states are different. Here we will show that this high-magnetic field behaviour is also correctly described by equation (3) if we consider the appropriate limits, and that we are able to reproduce this splitting of the cyclotron resonance peak and the collapse of the split resonance into a single peak with increasing Coulomb interaction.

We consider the above result and take the low-temperature limit, i.e. $1/\tau_{12} \approx 0$. In order to compare our result with those of others we further take the limit of zero dissipation, i.e. $1/\tau_i = 0$. Then the numerator of equation (4) reduces to

$$D(\omega) = -(\omega - \omega_{c,1})(\omega - \omega_{c,2}) + \left\{ n_1 m_1 (\omega - \omega_{c,1}) + n_2 m_2 (\omega - \omega_{c,2}) \right\} \frac{\omega_0}{n_1 m_1 + n_2 m_2} \tag{6}$$

which has the following zeros:

$$\omega\pm = \frac{1}{2} \left\{ (\omega_{c,1} + \omega_{c,2} + \omega_0) \pm \sqrt{(\omega_{c,1} + \omega_{c,2} + \omega_c)^2 - 4\left(\omega_{c,1}\omega_{c,2} + \omega_0 \frac{n_1 m_1 \omega_{c,1} + n_2 m_2 \omega_{c,2}}{n_1 m_1 + n_2 m_2} \right)} \right\} \tag{7}$$

and which results in two delta peaks in the absorption spectrum located at $\omega = \omega_\pm$. This result is exactly the one given by the simplified model of Cooper and Chalker [23] (see equations (9)–(11) of reference [23]). Cooper and Chalker used the following notations: $\delta\omega_c = \omega_{c,2} - \omega_{c,1}$, with the coupling strength $\alpha = \omega_0/\delta\omega_c$, the occupation of the minority carriers $p = n_1/(n_1 + n_2 m_2/m_1)$ and the shift in the CR frequency $\omega_{in}, \omega_{out} = (\omega_\pm - \omega_{c,2})/\delta\omega_c$. The coupling strength was calculated in reference [23] for the case of electrons localized on a Wigner lattice; it was found that $\alpha = 11.034(e^2 l^2/2\epsilon a^3)(1/\hbar\delta\omega_c)$ in the present cgs units; here ϵ is the static dielectric constant of the material, $l = \sqrt{\hbar c/eB}$ is the magnetic length and $a = \sqrt{2/\sqrt{3}n}$ is the lattice constant of the hexagonal Wigner lattice with n the electron density. Note that equation (7) is essentially the same as the one

obtained recently by Hu *et al* [24]. Both groups then introduced a Lorentzian broadening of these two peaks in order to compare the CR absorption with the experimental result. It should be noted that in our approach the broadening of the CR peak(s) is introduced in the initial stage of our phenomenological model and does not have to be added at the end of the calculation. A different approach was followed by Asano and Ando [25] who calculated numerically the energy levels of a finite rectangular system of electrons in a magnetic field with periodic boundary conditions. They used the Kubo formula in which (1) a thermal average was performed over the eigenvalues of the system, and (2) a Lorentzian broadening of the delta function expressing energy conservation was introduced.

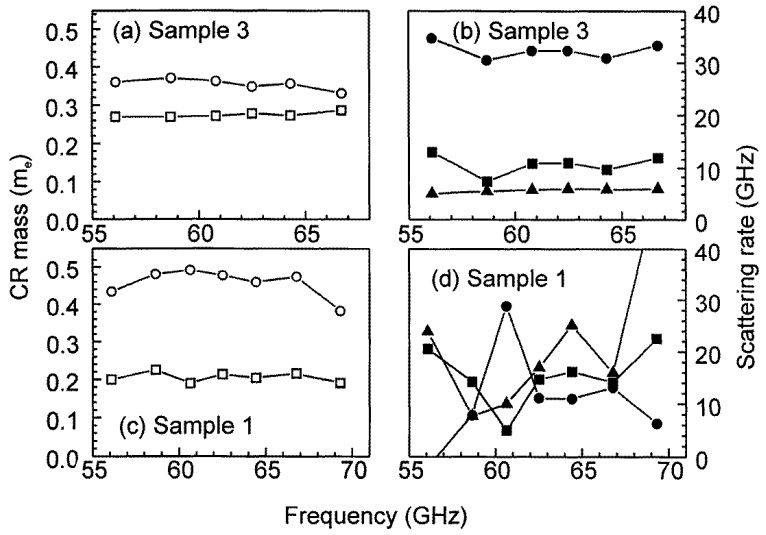

Figure 8. (a) Cyclotron resonance (CR) masses obtained by fitting the resonant cavity data at each frequency, at 500 mK, for sample 3. (b) Scattering rates (GHz) obtained from fitting 500 mK data for sample 3 ($1/\tau_i$, triangles; $1/\tau_{12}$, squares; $\omega_0/2\pi$, circles). (c) Cyclotron resonance masses obtained by fitting the resonant cavity data at each frequency, at 500 mK, for sample 1. (d) Scattering rates (GHz) obtained by fitting 500 mK data for sample 1 ($1/\tau_i$, triangles; $1/\tau_{12}$, squares; $\omega_0/2\pi$, circles).

5. Results of the fitting and discussion of the low-field data

In order to extract some further information about the underlying characteristics of the holes, we have fitted the experimental lineshapes using the above model. A difficulty in this procedure is the large number of parameters involved; in addition to intrinsic hole parameters such as the masses m_i $(i = 1, 2)$, the hole–lattice relaxation rates $1/\tau_i$ and the hole–hole relaxation rates $\omega_0/2\pi$ and $1/\tau_{12}$, we must take account of standing-wave-induced mixing between real and imaginary parts of $\sigma(\omega)$ (see section 2). If, for simplicity, it is assumed that $\tau = \tau_1 = \tau_2$, a value for τ somewhat shorter than that suggested by DC transport measurements is required in general to fit the observed cyclotron resonance lineshape. The difference is largest in the case of sample 3, where DC measurements suggest a mobility of 120 $m^2\ V^{-1}\ s^{-1}$ and the cyclotron resonance linewidth yields an AC mobility of $\sim$15 $m^2\ V^{-1}\ s^{-1}$. The insensitivity of DC measurements to small-angle scattering has been cited on a number of previous occasions [26] to explain the observed

differences between mobilities found in cyclotron resonance and DC transport. Thus we include τ as a free parameter in the fitting procedure.

Unique fits to the lineshape were obtained for sample 3 at 500 mK for six frequencies from 56.1 GHz to 66.7 GHz; for the two lowest frequencies measured, the second, higher-field resonance was insufficiently strong to obtain a reliable fit. The fits are shown as dotted lines in figure 6(a), and can be seen to follow the experimental curves very closely. The parameters obtained are plotted in figures 8(a) and 8(b); similar values for all of the parameters are obtained across this frequency range. The fits show that in the case of sample 3, the hole–hole interaction is dominated by $\omega_0/2\pi$ rather than $1/\tau_{12}$.

In contrast, although fits to the lineshapes for sample 1 at 500 mK (figure 6(b)) yield reasonable values for m_1 and m_2 (figure 8(c)), there was considerable scatter in the values of the various scattering rates (figure 8(d)); this may be associated with distortions to the lineshape caused by the quantum oscillations (see section 3). We have assumed no frequency dependence for the effective mass over this small frequency range and taken the two mean values obtained from this fitting for subsequent analysis of the temperature dependence data from sample 1, described below.

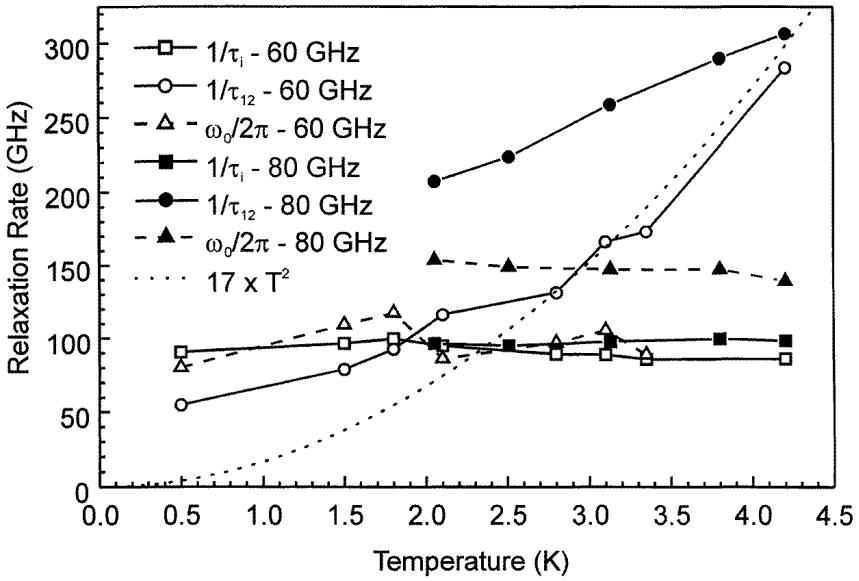

Figure 9. Hole–lattice, resistive hole–hole and reactive hole–hole scattering rates obtained from fitting resonant cavity data for sample 1 as a function of temperature (fitted lineshapes are shown in figure 5). Measurements at both 60 GHz and 80 GHz are shown and all fits assume masses of $0.21m_e$ and $0.46m_e$.

The temperature dependence of the hole–hole momentum relaxation rate has been obtained by fitting the cyclotron resonance data for sample 1 shown in figure 5 (fits shown as dotted lines). Masses of $m_1 = 0.21m_e$ and $m_2 = 0.46m_e$ are used throughout. This procedure yields roughly constant values for $1/\tau_i$ and $\omega_0/2\pi$. The temperature dependence of the lineshape is clearly due to $1/\tau_{12}$, which appears to increase superlinearly with temperature. Figure 9 shows the fitted relaxation rates and the function αT^2, with $\alpha \approx 17$ s^{-1} T^{-2} obtained by fitting to the values of $1/\tau_{12}$ measured at 60 GHz.

Figure 10(a) shows simulated cyclotron resonance lineshapes assuming that (1) $\omega_0/2\pi$

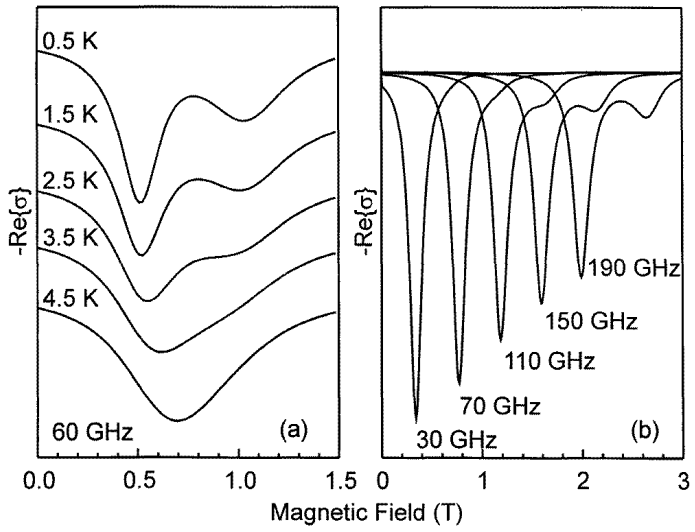

Figure 10. (a) The simulated cyclotron resonance temperature dependence of sample 1, obtained using the expression described in the text and assuming $1/\tau_{12} = 2.8T^2$. All other parameters are held constant: $\omega/2\pi = 60$ GHz, $m_1 = 0.21m_e$, $m_2 = 0.46m_e$, $1/\tau_1 = 1/\tau_2 = 94$ GHz, $n_2/n_1 = 1.75$, $\omega_0/2\pi = 75$ GHz. (b) The simulated cyclotron resonance frequency dependence of sample 3, obtained using the parameters found for this sample at 500 mK and 64.3 GHz: $m_1 = 0.28m_e$, $m_2 = 0.35m_e$, $1/\tau_1 = 1/\tau_2 = 38$ GHz, $n_2/n_1 = 1.1$, $\omega_0/2\pi = 200$ GHz, $1/\tau_{12} = 63$ GHz. Note that at 70 GHz the higher-field resonance is barely detectable in Re$\{\sigma\}$. However, it becomes visible in the measured spectra due to standing-wave-induced mixing of Im$\{\sigma\}$ into the measured signal.

is constant and (2) $1/\tau_{12} = \alpha T^2$ (see figure 9), in order to reproduce the qualitative features shown by sample 1 at 60 GHz. The parameter values are shown in the figure caption. Simulated cyclotron resonance lineshapes over a wider frequency range than that covered by the mm-wave experiment are shown in figure 10(b), using the parameters obtained for sample 3 at 64.3 GHz and 500 mK. Note that in this figure the imaginary component of $\sigma(\omega)$ has been removed with the result that the high-field satellite resonance is no longer visible below 1 T but grows in strength at higher magnetic fields above this value. The lower-field resonance decreases in strength at higher frequencies as part of its oscillator strength transfers to the higher-field resonance.

The fitted hole masses for sample 1 are in reasonable agreement with subband calculations for a (311) accumulation layer with $p_s = 3 \times 10^{15}$ m^{-2}. The calculations start from a rotated Luttinger Hamiltonian for a general [hkk] growth direction [27] and use an approximate potential obtained by solving the Poisson equation using a Fang–Howard wavefunction in a triangular potential well. It is known that the difference between the latter approximation and fully self-consistent calculations is insignificant [28, 29]. The hole subbands are derived in the envelope-function approximation and the axial approximation is invoked. The hole potential was found to be particularly sensitive to the nature and level of background doping in the GaAs and so calculations were performed for both inversion and accumulation layer cases. Since the dominant impurities, silicon and carbon, both act as acceptors in this crystal orientation, the background doping is expected to be p type; the fitted values for m_1 and m_2 reinforce this view. The masses calculated at the Fermi energy are $m_1 = 0.16m_e$, $m_2 = 0.48m_e$ and $m_1 = 0.16m_e$, $m_2 = 0.35m_e$ for the accumulation and

inversion cases respectively. For more quantitative agreement, axial asymmetry must be included in the subband calculation [28].

The measured splitting between m_1 and m_2 found in the lower-density sample, 3, is somewhat less than that expected from subband calculations. These suggest $m_1 = 0.15m_e$ and $m_2 = 0.34m_e$, whereas it is found that $m_1 = 0.28m_e$ and $m_2 = 0.35m_e$ give the best fit to the data. The rather small difference in masses between the spin subbands is further experimentally reinforced by transport measurements of the subband hole densities [30] which indicate $n_2/n_1 \simeq 1.1$ for samples with $p_s = 0.8 \times 10^{15}$ m^{-2}, and hence broadly similar masses for the two subbands.

DC transport has also been used to probe the hole–hole scattering rate $1/\tau_{12}$ through studies of the low-field positive longitudinal magnetoresistance found in these samples [30, 31]. The longitudinal resistance, $R_{xx} = \mathrm{Re}\{\sigma_0\}/|\sigma_0|$, may be modelled using the zero-frequency limit of the dynamical conductivity, $\sigma(\omega)$, given in equation (3) derived in section 4. The positive magnetoresistance arises from the presence of two carrier types of different mobility; this may occur through either a difference in mass or a difference in scattering times between the populations. $1/\tau_{12}$ influences the magnetoresistance by relaxing the relative momenta, or equivalently the mobility, of the two groups of holes as discussed above, leading to zero magnetoresistance in the case of strong hole–hole scattering. The temperature dependence of the magnetoresistance may then provide information on the temperature dependence of $1/\tau_{12}$. DC measurements of R_{xx} provide no information on the reactive part of the hole–hole interaction since $\mathrm{Re}\{\sigma\}$ has no ω_0-dependence at $\omega = 0$. A (100) sample with $p_s = 3.2 \times 10^{15}$ m^{-2} was studied by Murzin *et al* [31]; a T^2-dependence for $1/\tau_{12}$ and constant hole–lattice relaxation rates are assumed. By fitting the temperature dependence of the magnetoresistance the $1/\tau_{12}$ prefactor was found to be 50 GHz K^{-2}. This implies hole–hole scattering rates of very similar size to those obtained for sample 1 in this report. A different magnetoresistance study, by Crump [30], considered samples with $p_s = 0.9$ and 1.75×10^{15} m^{-2} over the temperature range 0.3–1.5 K; in Crump's work the single-particle relaxation rates were fitted at each temperature. The temperature dependence of $1/\tau_{12}$ was found to be very weak; the strong temperature dependence of the low-field magnetoresistance was attributed to an increase in the hole–lattice scattering rate of the lighter subband through temperature-dependent screening [30].

The T^2-dependence of inter-particle Coulomb scattering is well known theoretically and has been tested experimentally through transport measurements on double-layer systems [32]. It is perhaps therefore surprising that our measurements apparently indicate a significant value of $1/\tau_{12}$ at the lowest temperatures. Appel and Overhauser [16] have pointed out that $1/\tau_{12}$ has a term proportional to $\hbar\omega^2$, independent of temperature. However, this is insufficient to explain the low-temperature limit of $1/\tau_{12(T=0)} = 50.3$ GHz.

The apparent increase in the $1/\tau_{12}$ obtained at 80 GHz compared to that at 60 GHz probably has a different origin; the reduced splitting at 2 K may be due to the 'diamagnetic' effect of the larger field which tends to reduce the distinction between the two spin subbands at smaller filling factors [33]. The latter effect would also affect the results at 60 GHz and may explain the difference between experimental masses and those obtained from model calculations.

We obtain a value of $1/\tau_{12} = 310$ GHz for sample 1 at 4.2 K; this is considerably larger than that calculated for a Si inversion layer with electron density $n_s = 5 \times 10^{15}$ m^{-2} and similar Fermi energies in each subband by Ting *et al* [20], who found $1/\tau_{12} \simeq 25$ GHz at 10 K. Conversely, the reactive scattering rates appear quite similar for the two-dimensional hole system and the Si MOSFETs; $\omega_0/2\pi \simeq 120$ GHz was calculated for the Si case at 10 K compared to $\omega_0/2\pi \simeq 88$ GHz measured for sample 1 at 3 K. Although $1/\tau_{12}$ is

more significant at lower carrier density, the larger value found in the two-dimensional hole system may arise from the additional scattering processes which are possible compared to the Si case; since the electron subbands in Si MOSFETs lie in pockets widely separated in wavevector space, exchange of carriers between the subbands is much more difficult. In the hole system, the two hole Fermi cylinders are coaxial and concentric, so spin-flip scattering is allowed through subband mixing.

In samples of lower hole density a single Lorentzian resonance is obtained down to low temperatures as a result of the stronger hole–hole interaction and the smaller difference in hole masses between spin subbands at lower Fermi energies. In all theories for interacting systems, the hole–hole interactions may not alter the mean effective mass of the system; the strong temperature dependence of the mean mass, observed where a single, sharp resonance occurs, is attributed to the strong non-parabolicity of the hole subband. The density of states increases with energy, and this will weight the effective mass to a higher value at higher temperatures. The chemical potential is only weakly dependent on temperature for $kT \ll E_F$. However in the limit $kT \gg E_F$ we have $\mu \propto -kT \ln(kT)$. Thus the temperature dependence may be enhanced in samples of small p_s.

6. Summary and conclusions

Observations of cyclotron resonance have demonstrated that inter-particle interactions are very significant in the two-dimensional hole system. For a system of two interacting Fermi liquids, under the conditions $\hbar\omega_c \ll kT \ll E_F$, the coupling between the two liquids is characterized by a complex relative momentum relaxation time. We have solved the classical kinetic equations for such a two-component system in order to fit the measured cyclotron resonance lineshapes obtained from the two-dimensional hole system. In the hole system the two populations of different mass are formed from the zero-field 'spin splitting' of the heterojunction subbands. The hole–hole relaxation rates are found to lie in the GHz region in the low-field case; if the difference in cyclotron frequency of the two hole populations is much smaller than the hole–hole scattering rate a single coupled resonance occurs, whereas if it is much greater, single-particle behaviour is observed. By fitting the experimental data we have extracted the hole effective masses and scattering rates. The real component of the hole–hole scattering rate is expected to vanish at zero temperature; we find that the hole–hole relaxation rate is dominated by $\omega_0/2\pi$ at 500 mK in our samples, corresponding to the reactive component of the interaction between the two hole populations. As the temperature is raised the dissipative part of the hole–hole relaxation rate, $1/\tau_{12}$, increases superlinearly. A qualitatively similar temperature dependence can be reproduced assuming a T^2-dependence of $1/\tau_{12}$, although more detailed fitting suggests a non-zero value of $1/\tau_{12}$ at zero temperature. $\omega_0/2\pi$ acts to renormalize the hole masses and oscillator strengths; no significant temperature dependence for this quantity was observed over the ranges investigated. The strong temperature dependence of the mean effective mass found at mm-wave frequencies is attributed to non-parabolicity of the hole subbands and is found for all samples with sufficiently narrow cyclotron resonance linewidths.

Acknowledgments

This work was supported by the EPSRC (UK), the Royal Society (UK), the European Union Human Capital and Mobility Initiative and the Belgian National Science Foundation.

References

[1] Hawksworth S J, Hill S, Janssen T J B M, Chamberlain J M, Singleton J, Ekenberg U, Summers G M, Davies G A, Nicholas R J, Valadares E C, Henini M and Perenboom J A A J 1993 *Semicond. Sci. Technol.* **8** 1465

[2] Harrison P A, Hayden R K, Henini M, Valadares E C, Hughes O H and Eaves L 1992 *J. Vac. Sci. Technol.* B **10** 2040

[3] Hill S, Cole B E, Chamberlain J M, Singleton J, Rodgers P J, Janssen T J B M, Pattenden P A, Gallagher B L, Hill G and Henini M 1995 *Physica* B **211** 440

[4] Störmer H L, Schlesinger Z, Chang A, Tsui D C, Gossard A C and Wiegmann W 1983 *Phys. Rev. Lett.* **51** 126
Hirakawa K, Zhao Y, Santos M B, Shayegan M and Tsui D C 1993 *Phys. Rev.* B **47** 4076 and references therein

[5] Davies G A 1989 *PhD Thesis* University of Cambridge

[6] The second paper in this pair [7] will present cyclotron resonance data in the very high-field limit ($B \sim 40$ T) which also show evidence for strong hole–hole correlations. The different relative sizes of $\hbar\omega_c$, E_F and kT mean that the data in reference [7] behave rather differently to those in the current paper. Nevertheless, it will be shown that the model which we have developed (see section 4) can also be used to treat the high-field cyclotron resonance spectra [7].

[7] Cole B E, Batty W, Singleton J, Chamberlain J M, Li L, van Bockstal L, Imanaka Y, Shimamoto Y, Miura N, Peeters F M, Henini M and Cheng T 1997 *J. Phys.: Condens. Matter* at press

[8] Henini M, Rodgers P J, Crump P A, Gallagher B L and Hill G 1995 *J. Cryst. Growth* **150** 446

[9] Goy P 1989 *French Patent No* CNRS-ENS
Gross M 1992 *US Patent No* 5 119 035

[10] Poole C P Jr 1967 *Electron Spin Resonance* (New York: Interscience)

[11] The somewhat asymmetric lineshapes in figure 1(c) are a consequence of the transmission configuration used, in which the influence of standing waves in the waveguides is unavoidable. The traces in figure 1(c) have been scaled to a similar size since the absolute magnitude of the cyclotron resonance depends strongly on the sample position relative to the standing-wave mode structure and is not consistent between samples and frequencies.

[12] A comprehensive description of such effects is given by
Nicholas R J 1994 *Optical Properties of Semiconductors (Handbook on Semiconductors 2)* ed T S Moss and M Balkanski (Amsterdam: North-Holland) section 3, ch 7

[13] Hill S O 1994 *DPhil Thesis* University of Oxford

[14] See
Horst M, Merkt U and Germanova K G 1985 *J. Phys. C: Solid State Phys.* **18** 1025
See also reference [12], chapter 7.

[15] Abstreiter G, Koch J F, Goy P and Couder Y 1976 *Phys. Rev.* B **14** 2494
Abstreiter G 1980 *Surf. Sci.* **98** 413
Allen J S, Tsui D C and Dalton J V 1974 *Phys. Rev. Lett.* **32** 107
Kotthaus J P, Abstreiter G and Koch J F 1976 *Solid State Commun.* **15** 517
Kühlbeck H and Kotthaus J P 1975 *Phys. Rev. Lett.* **35** 1019
Stallhofer P, Kotthaus J P and Koch J F 1976 *Solid State Commun.* **20** 519
Kennedy T A, Wagner R J, McCombe B D and Tsui D C 1976 *Surf. Sci.* **58** 185

[16] Appel J and Overhauser A W 1978 *Phys. Rev.* B **18** 758

[17] Kohn W 1961 *Phys. Rev.* **123** 1242

[18] Peeters F M 1990 *Phys. Rev.* B **42** 1486

[19] Kukkonen C A and Maldague P F 1976 *Phys. Rev. Lett.* **37** 782

[20] Ting C S 1980 *Surf. Sci.* **98** 437
Ting C S, Ganguly A K, and Lai W Y 1981 *Phys. Rev.* B **24** 3371

[21] Takada Y and Ando T 1978 *J. Phys. Soc. Japan* **44** 905
Takada Y 1980 *Surf. Sci.* **98** 442

[22] Besson M, Gornik E, Englehardt C M and Weimann G 1992 *Semicond. Sci. Technol.* **7** 1274
Michels J G, Hill S, Warburton R J, Summers G M, Gee P, Singleton J, Nicholas R J, Foxon C T and Harris J J 1994 *Surf. Sci.* **305** 33
Michels J G, Daly M S, Gee P, Hill S, Nicholas R J, Singleton J, Summers G M, Warburton R J, Foxon C T and Harris J J 1996 *Phys. Rev.* B **54** 13 807

[23] Cooper N R and Chalker J T 1994 *Phys. Rev. Lett.* **72** 2057

[24] Hu C M, Friedrich T, Batke E, Köhler K and Ganser P 1995 *Phys. Rev.* B **52** 12 090
[25] Asano K and Ando T 1996 *J. Phys. Soc. Japan* **65** 1191
[26] See reference [12], chapter 7, and references therein.
See also
Kusters R M, Wittekamp F A, Singleton J, Perenboom J A A J, Jones G A C, Ritchie D A, Frost J E F and Andre J-P 1992 *Phys. Rev.* B **46** 10 207 and references therein
[27] Cole B E, Batty W, Imanaka Y, Shimamoto Y, Singleton J, Chamberlain J M, Miura N, Henini M and Cheng T 1995 *J. Phys.: Condens. Matter* **7** L675
[28] Batty W, Cole B, Singleton J and Chamberlain J M 1997 to be published
[29] Ekenberg U 1996 private communication
[30] Crump P 1996 *PhD Thesis* University of Nottingham
[31] Murzin S S, Dorozhkin S I, Landwehr G and Gossard A C 1996 *Proc. 23rd Int. Conf. on the Physics of Semiconductors (Berlin, 1996)* vol 3, ed M Scheffler and R Zimmerman (Singapore: World Scientific) p 2187
[32] See
Rubel H, Linfield E H, Hill N P R, Nicholls J T, Ritchie D A, Brown K M, Pepper M and Jones G A C 1996 *Surf. Sci.* **361+362** 134 and references therein
[33] Ekenburg U and Altarelli M 1985 *Phys. Rev.* B **32** 3712